Neuron

VTA Glutamate Neuron Activity Drives Positive Reinforcement Absent Dopamine Co-release

Graphical Abstract

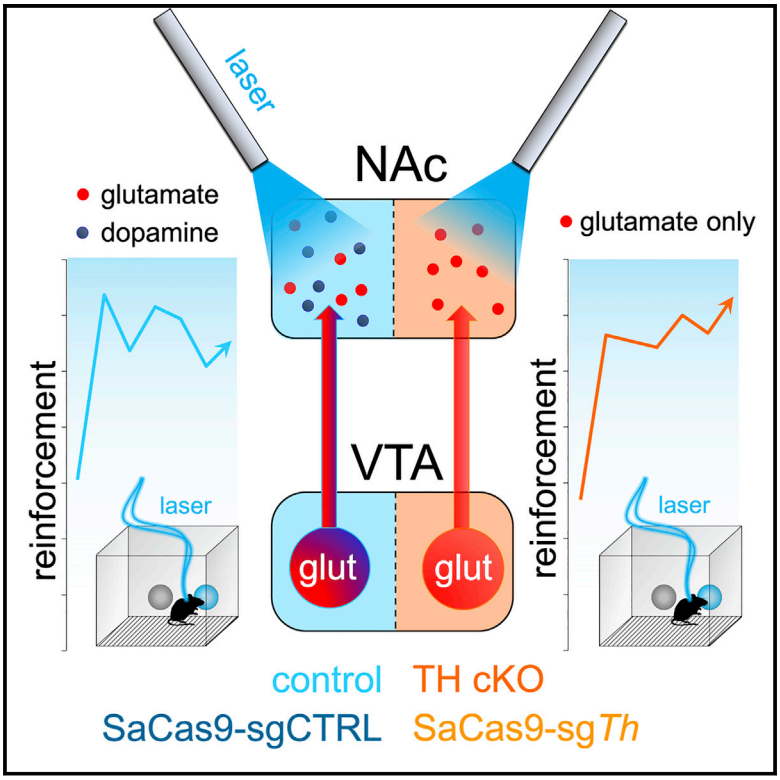

Highlights

- Activation of VTA glutamate neurons can reinforce behavior
- Activation of VTA glutamate neurons also leads to dopamine (DA) release
- We generated two distinct models to abolish this coincident DA signal
- VTA glutamate neuron activity can serve as a reinforcer independent from DA

Authors

Vivien Zell, Thomas Steinkellner, Nick G. Hollon, ..., Xin Jin, Larry S. Zweifel, Thomas S. Hnasko

Correspondence

thnasko@health.ucsd.edu

In Brief

Activation of VTA glutamate neurons leads to dopamine co-release in nucleus accumbens. Zell et al. genetically block this dopamine signal to show that VTA glutamate projections to nucleus accumbens can reinforce behaviors independently. These findings establish a parallel dopamine-independent mesolimbic pathway capable of supporting positive reinforcement.

Zell et al., 2020, Neuron *107*, 1–10
September 9, 2020 Published by Elsevier Inc.
https://doi.org/10.1016/j.neuron.2020.06.011

Please cite this article in press as: Zell et al., VTA Glutamate Neuron Activity Drives Positive Reinforcement Absent Dopamine Co-release, Neuron (2020), https://doi.org/10.1016/j.neuron.2020.06.011

Neuron

CellPress

Report

VTA Glutamate Neuron Activity Drives Positive Reinforcement Absent Dopamine Co-release

Vivien Zell,[1] Thomas Steinkellner,[1] Nick G. Hollon,[2] Shelley M. Warlow,[1] Elizabeth Souter,[1] Lauren Faget,[1] Avery C. Hunker,[3] Xin Jin,[2] Larry S. Zweifel,[3] and Thomas S. Hnasko[1,4,5,*]

[1]Department of Neurosciences, University of California, San Diego, La Jolla, CA 92093, USA
[2]Molecular Neurobiology Laboratory, The Salk Institute for Biological Studies, La Jolla, CA 92037, USA
[3]Department of Pharmacology, University of Washington, Seattle, WA 98195, USA
[4]Research Service VA San Diego Healthcare System, San Diego, CA 92161, USA
[5]Lead Contact
*Correspondence: thnasko@health.ucsd.edu
https://doi.org/10.1016/j.neuron.2020.06.011

SUMMARY

Like ventral tegmental area (VTA) dopamine (DA) neurons, VTA glutamate neuron activity can support positive reinforcement. However, a subset of VTA neurons co-release DA and glutamate, and DA release might be responsible for behavioral reinforcement induced by VTA glutamate neuron activity. To test this, we used optogenetics to stimulate VTA glutamate neurons in which tyrosine hydroxylase (TH), and thus DA biosynthesis, was conditionally ablated using either floxed *Th* mice or viral-based CRISPR/Cas9. Both approaches led to loss of TH expression in VTA glutamate neurons and loss of DA release from their distal terminals in nucleus accumbens (NAc). Despite loss of the DA signal, optogenetic activation of VTA glutamate cell bodies or axon terminals in NAc was sufficient to support reinforcement. These results suggest that glutamate release from VTA is sufficient to promote reinforcement independent of concomitant DA co-release, establishing a non-DA mechanism by which VTA activity can support reward-seeking behaviors.

INTRODUCTION

The ventral tegmental area (VTA) has a pivotal role in the control of motivated behaviors. Dopamine (DA) transmission from VTA to nucleus accumbens (NAc) and other limbic structures contributes to the processes underlying motivated behavior and behavioral reinforcement and is a key structure for the initiation of drug addiction (Ikemoto and Bonci, 2014). DA release from VTA neurons is sufficient to support positive reinforcement, reward learning, and to invigorate reward seeking; thus, DA release is often conceptualized as a primary reward signal (Berridge et al., 2009; Fields et al., 2007; Keiflin and Janak, 2015). However, increasing evidence has established important functional and physiological roles for non-DA neurons in VTA, including those that release glutamate or GABA (Bariselli et al., 2016; Pupe and Wallén-Mackenzie, 2015). Further complexity is added by the fact that some VTA neurons co-release multiple neurotransmitters (Hnasko and Edwards, 2012; Trudeau et al., 2014).

Approximately 36% of NAc-projecting VTA neurons express the type-2 vesicular glutamate transporter (VGLUT2) (Yamaguchi et al., 2011), and electrophysiological data demonstrate that essentially all medium spiny neurons (MSNs) in medial NAc shell receive glutamatergic input from VTA (Hnasko et al., 2012; Mingote et al., 2015, 2019; Stuber et al., 2010; Yoo et al., 2016) as do striatal cholinergic interneurons (Cai and Ford, 2018; Chuhma et al., 2014, 2018). Optogenetic activation of VTA glutamate cell bodies or terminals in NAc can support self-stimulation (Wang et al., 2015; Yoo et al., 2016), but their activation has also been shown to drive apparent avoidance in some behavioral assays (Qi et al., 2016; Yoo et al., 2016). This avoidance behavior might be a paradoxical consequence resulting from a preference for short duration trains of VTA glutamate neuron stimulation (Yoo et al., 2016). Alternatively, glutamate release from VTA terminals in NAc might drive avoidance through preferential activation of NAc interneurons, even though DA co-release from a subset of these neurons contributes to reward (Qi et al., 2016). Thus, it remains unclear whether the reward signals supporting self-stimulation of VTA glutamate neurons are mediated by glutamate per se, or by the concomitant co-release of DA.

Here, we tested whether VTA glutamate projections to NAc drive reward independently of DA co-release. We generated conditional knockout (cKO) mice in which *Tyrosine hydroxylase* (*Th*) was specifically knocked out from VGLUT2-expressing neurons to disrupt DA synthesis. Optogenetic stimulation of VTA glutamate neurons or their axon terminals led to robust DA release in NAc of controls but not cKO mice. Further, while cKOs displayed only a minor reduction in basal locomotor activity, loss of DA co-release did not abolish or otherwise impact self-stimulation or other measures of behavioral reinforcement. To overcome potential compensatory adaptations associated with the loss of Th from

Please cite this article in press as: Zell et al., VTA Glutamate Neuron Activity Drives Positive Reinforcement Absent Dopamine Co-release, Neuron (2020), https://doi.org/10.1016/j.neuron.2020.06.011

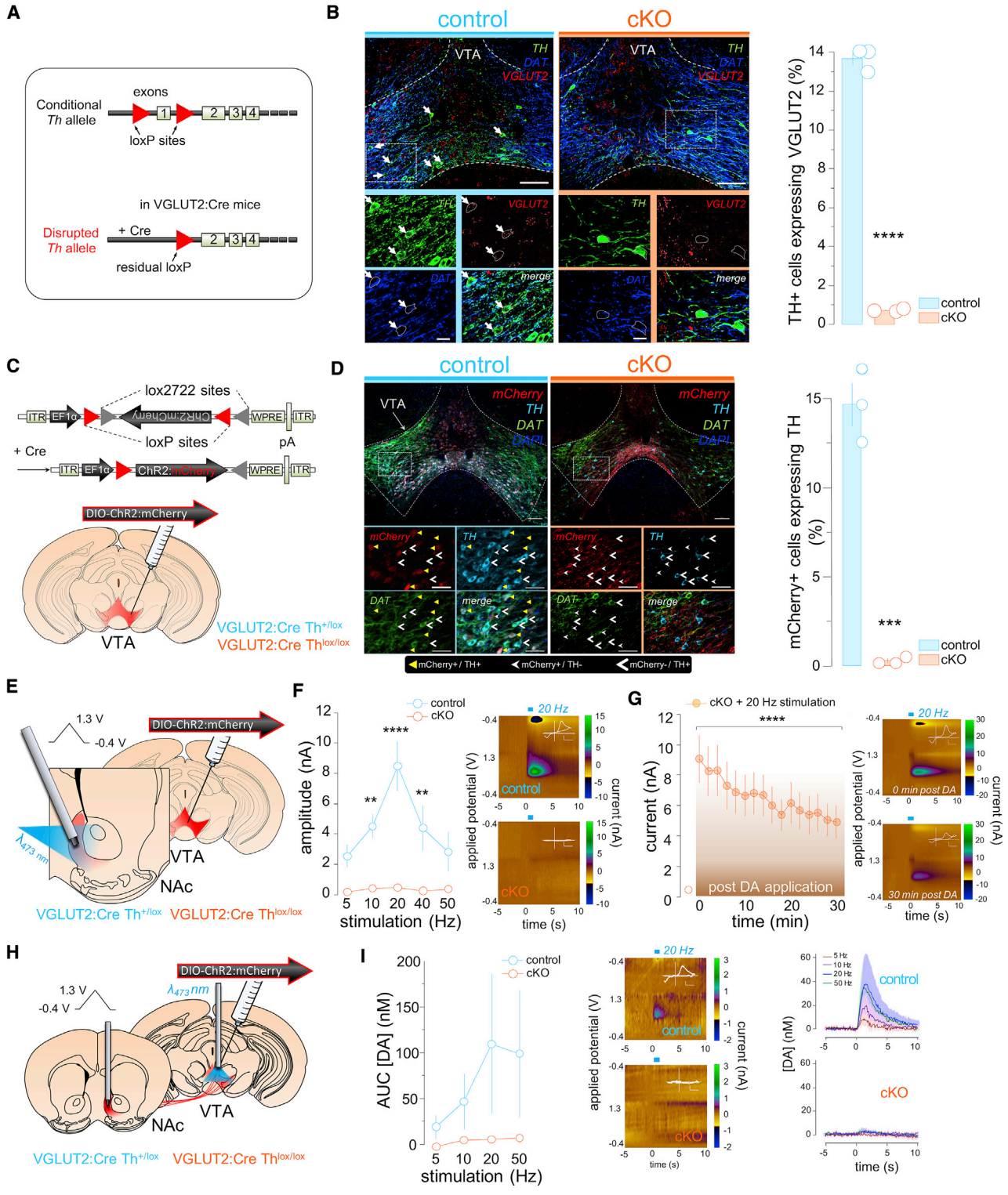

Figure 1. Disruption of TH Expression and DA Release from VTA Glutamate Neurons

(A) Genetic disruption of floxed *Th* gene in *Slc17a6*^{Cre} (VGLUT2-Cre) mice.

(B) Coronal sections through VTA labeled with antibodies against TH and dopamine transporter (DAT), plus RNAscope probes targeting VGLUT2 transcripts. Neurons co-expressing TH and VGLUT2 (arrows) in controls were virtually absent in cKO; scale, 500 μm (top) and 100 μm (bottom); t test, ****$p < 0.0001$ (n = 3 mice/group).

(legend continued on next page)

Please cite this article in press as: Zell et al., VTA Glutamate Neuron Activity Drives Positive Reinforcement Absent Dopamine Co-release, Neuron (2020), https://doi.org/10.1016/j.neuron.2020.06.011

VTA glutamate neurons during development, we also implemented a virus-based CRISPR/Cas9 approach to disrupt Th expression and DA release from VTA glutamate neuron in adult mice, to similar effect. Together, our results indicate that VTA glutamate neuron activity can support robust behavioral reinforcement independent of their ability to recruit DA release.

RESULTS

Conditional Ablation of DA Synthesis in VTA Glutamate Neurons

To test the contribution of DA co-transmission to VTA glutamate neuron function, we generated mice with conditional deletion of *Th* (Darvas and Palmiter, 2010) selectively in VGLUT2-Cre-expressing neurons (Figure 1A). Brain sections from cKO (*Slc17a6*$^{+/Cre}$; *Th*$^{lox/lox}$), and heterozygous control littermates (control: *Slc17a6*$^{+/cre}$; *Th*$^{+/lox}$) were used to confirm the loss of TH in VTA glutamate neurons. Using a combination of *in situ* hybridization and immunohistochemistry, we found that ~14% of neurons expressing VGLUT2 mRNA were also TH^{+} in control mice, whereas TH^{+} VGLUT2 neurons were essentially absent in the VTA of cKO mice (Figure 1B). Although numerous studies demonstrate that 10%–20% of VTA DA neurons express VGLUT2 in the adult, a much higher proportion transiently express VGLUT2 during development (Bérubé-Carrière et al., 2009; Kouwenhoven et al., 2019; Mendez et al., 2008; Steinkellner et al., 2018). As a consequence, we observed ~80% decrease in the number of TH-immunoreactive cell bodies in both VTA and SNc of cKOs (Figures S1A and S1B). We also observed a corresponding decrease in TH-immunoreactive DA axon terminals in the NAc, and caudate/putamen (CPu) (Figures S1C and S1D). In contrast, DA transporter (DAT) immunoreactivity was unaltered, indicating that DA neuronal architecture was intact in cKO mice. Despite the reduced TH expression, we observed only a modest reduction in baseline locomotor activity in cKO mice, and locomotor responses to L-DOPA, amphetamine, or the D1R agonist SKF81297 were similar between cKO and control mice, suggesting intact psychomotor function (Figure S2).

Disruption of DA Transmission from VTA Glutamate Neurons

To control VTA glutamate neuron activity, we infused an adeno-associated virus (AAV) engineered for Cre-dependent expression of Channelrhodopsin-2:mCherry (ChR2:mCherry) into the medial VTA of control and cKO mice (Figure 1C). Approximately 15% of mCherry^{+} VTA glutamate cell bodies co-labeled with TH in control mice, but co-expressing cells were virtually absent in cKOs, further confirming the conditional loss of TH from VGLUT2^{+} VTA neurons (Figure 1D).

To test whether the loss of TH from VTA glutamate neurons was sufficient to abolish evoked DA release, we used fast-scan cyclic voltammetry (FSCV) in brain slices through the medial NAc shell (Figure 1E). Optogenetic stimulation of VTA glutamate terminals in the NAc produced a robust frequency-dependent increase in evoked DA in controls but not the cKO (Figure 1F). However, bath application of DA (10 μM, 10 min) rescued ChR2-evoked DA transients in cKOs (Figure 1G), demonstrating that VTA glutamate terminals retain the capacity to release DA when substrate is available.

Importantly, we also demonstrate that DA release is absent following optogenetic stimulation of VTA glutamate neurons *in vivo*. In this experiment, ChR2 was expressed in VTA glutamate neurons, optic fibers were implanted in VTA, and carbon fibers were implanted in medial NAc (Figures 1H and S4). Optogenetic stimulation (1 s) elicited frequency-dependent DA release in control but not cKO mice (Figure 1I). Together, these results demonstrate the functional loss of NAc DA release in cKO mice upon optogenetic stimulation of VTA glutamate neurons.

VTA Glutamate Transmission Is Similar at Both D1 and D2 MSNs and Is Intact in cKO

To test whether glutamate release was altered in cKO mice, we measured excitatory postsynaptic currents (oEPSCs) evoked by optogenetic stimulation of VTA glutamate terminals in NAc (Figure S3A). We found 6,7-dinitroquinoxaline-2,3(1H,4H)-dione (DNQX)-sensitive oEPSCs of similar amplitude in cKO and control mice (Figure S3B), suggesting that, unlike DA release, glutamate transmission was intact. We also measured paired-pulse ratios (PPRs) and found substantial paired-pulse depression in both genotypes, though depression was reduced in the cKO (Figure S3C), which could be due to reduced DA auto-receptor activation at these excitatory pre-synaptic terminals (Adrover et al., 2014; Chuhma et al., 2009). The onset delay and deactivation time constant (τ) of oEPSCs did not differ across genotypes (Figure S3D).

D1- and D2-type MSNs comprise >95% of NAc neurons but have distinct functional roles (Cole et al., 2018; Kravitz et al., 2012; Lobo and Nestler, 2011; Thibeault et al., 2019). To test whether VTA glutamate neurons might preferentially impact

(C) Strategy for selective expression of ChR2:mCherry in VGLUT2 VTA neurons.
(D) Coronal sections show colocalization of TH and ChR2:mCherry is nearly absent in the cKO; scale, 100 μm (top) and 50 μm (bottom); t test, ***p = 0.0003 (n = 3 mice/group).
(E) Schematic of *ex vivo* FSCV to measure DA evoked from VTA glutamate terminals.
(F) Photostimulation elicited frequency-dependent DA transients in the medial NAc shell in control but not cKO; RM two-way ANOVA, main effect of frequency, $F_{(4, 28)} = 11.0$, $p < 0.0001$; genotype, $F_{(1, 7)} = 22.5$, $p = 0.002$ and interaction, $F_{(4,28)} = 9.6$, $p < 0.0001$. Sidak's multiple comparisons test ****p < 0.0001, **p < 0.01 (control n = 4, cKO n = 5 mice). Right insets show example color plots following 20 Hz photostimulation. Voltammogram scale: 2 nA; 0.3 V.
(G) Bath application of DA (10 μM, 10 min) rescued opto-triggered DA transients in cKO; RM one-way ANOVA, main effect of treatment, $F_{(16, 64)} = 17.5$, $p < 0.0001$ (n = 5 mice). Bonferroni's multiple comparisons test ****p < 0.0001. Right insets show example color plots following 20 Hz photostimulation at 0 (top) and 30 (bottom) min after DA bath application/wash. Voltammogram scale: 2 nA; 0.3 V.
(H) Schematic of *in vivo* FSCV to measure evoked DA from VTA glutamate terminals.
(I) Photostimulation of VTA glutamate cell bodies elicited frequency-dependent DA signals in NAc; Friedman test, main effect of frequency in controls, $p < 0.0001$ (n = 4 mice) but not cKO mice, $p = 0.43$ (n = 5). Voltammogram scale: 1 nA; 0.3 V.
Data are represented as mean ± SEM. See also Figures S1–S4.

Please cite this article in press as: Zell et al., VTA Glutamate Neuron Activity Drives Positive Reinforcement Absent Dopamine Co-release, Neuron (2020), https://doi.org/10.1016/j.neuron.2020.06.011

these sub-populations, we used D1R-Cre × VGLUT2-Cre or A2a-Cre × VGLUT2-Cre double-transgenic mice to achieve conditional expression of (1) ChR2:EYFP in VTA VGLUT2 neurons and (2) mCherry in D1 or D2 (A2a) subtype-defined NAc MSNs (Figure S3E). To our knowledge, there is no VGLUT2 expressing neurons in the NAc nor D1R or A2a expressing neurons in VTA, cf. Allen Brain Atlas: Slc17a6 (73818754), Drd1 (352), and Adora2a (72109410) (Lein et al., 2007). We observed oEPSCs at both MSN types, and no significant difference was detected between $D1R^+$ versus putative $D1R^-$ nor $A2a^+$ versus putative $A2a^-$ neurons (Figure S3F). PPR, delay, and τ were also unchanged across MSN subtypes (Figures S3G and S3H). Together these results show that VTA glutamate neurons do not make preferential contact onto D1-type compared to D2-type projecting MSNs.

Self-stimulation of VTA Glutamate Neurons in the Absence of DA Co-release

Previous work from our lab demonstrated that optogenetic activation of VTA glutamate cell bodies or their terminals in NAc can support intracranial self-stimulation (ICSS) (Wang et al., 2015; Yoo et al., 2016). Curiously, mice that self-stimulated these neurons in an operant task showed a counter-intuitive frequency-dependent avoidance for their stimulation in a real-time place preference (RTPP) assay. However, this apparent avoidance was accompanied by an increased rate of entries into the active side and a preference for short duration trains of VTA glutamate neuron stimulation (Yoo et al., 2016). While these data imply distinct functional roles for VTA DA and glutamate neurons in positive reinforcement, optogenetic activation of VTA glutamate neurons also increases DA signaling in NAc (Figure 1) through transmitter co-release and/or local excitatory synapses onto VTA DA neurons (Dobi et al., 2010; Qi et al., 2016; Yoo et al., 2016). Therefore, to test the contribution of DA to behavioral reinforcement driven by VTA glutamate neurons, we performed ICSS and RTPP using cKO mice that lack the ability to synthesize and co-release DA.

ChR2:mCherry or mCherry was expressed in VTA glutamate neurons in control and cKO mice, and optic fibers were bilaterally implanted dorsal to medial NAc shell to target axon terminals. Mice were first tested on a 2-hole ICSS assay where nosepokes on hole "A" (active) triggered a laser to deliver a 1 s 40-Hz stimulus, while nosepokes on hole "B" (inactive) were without effect (Figure 2A). This frequency and pattern of stimulation was selected because prior works show that mice can discriminate and show preference for it and because VTA glutamate neurons can fire at similar frequency in response to salient stimuli (Root et al., 2018a; Wang et al., 2015; Yoo et al., 2016). Across the first 4 test sessions mice displayed strong preference for the active hole with no significant differences detected between genotypes (Figures 2B). Over the subsequent 4 sessions holes "A" and "B" were swapped, and both genotypes switched their preference to engage with the active hole; mCherry-expressing control mice did not show a preference or a switch and performed few nosepokes (Figures 2B and 2C). We also tested a separate cohort of animals with optic fibers implanted dorsal to VTA glutamate cell bodies rather than NAc terminals (Figure 2D); these animals also displayed a robust preference for the active nosepoke with no difference between genotype (Figures 2E and 2F).

We next tested mice in the RTPP procedure where they were provided free access to two compartments: entrance into active side A-triggered 40-Hz optogenetic stimulation that discontinued upon entry into side B (Figure 3A). When targeting VTA glutamate fibers in NAc, both genotypes spent less time in the active chamber and switched their side preference to the inactive chamber when side B was switched to active; mCherry-expressing mice showed no significant preference or avoidance (Figure 3B). Both genotypes also showed an increased approach rate into the active side compared to mCherry-expressing mice (Figure 3C), and there was no significant difference between controls and cKO mice that lack the evoked DA signal. Mice with implants dorsal to VTA were used to target the cell bodies (Figure 3D) and displayed similar patterns of active side avoidance (Figure 3E), with increased approach rates over time (Figure 3F), and no effect of genotype on these behaviors. Together, these results demonstrate that VTA glutamate neuron activation can drive self-stimulation and approach behavior in the absence of concomitant DA co-release, suggesting VTA glutamate neurons represent a DA-independent mesolimbic reward circuit.

CRISPR/Cas9 Disruption of DA Transmission from VTA Glutamate Neurons

While the above data suggest that VTA glutamate neurons can convey a reinforcement signal that does not depend on increased DA release, the disruption of DA synthesis and release included neurons that do not express VGLUT2 in the adult due to transient developmental expression of VGLUT2 in a wider population of midbrain DA neurons (Figure S1). Further, loss of TH from early development might cause compensatory adaptations in cKO mice. To bypass these issues, we turned to a recently developed viral-based CRISPR/Cas9 approach to disrupt DA synthesis and release selectively from adult VTA neurons that express VGLUT2. This approach relied on a single AAV vector for Cre-dependent expression of *Staphylococcus aureus* Cas9 (SaCas9) and U6 promoter-driven expression of a single-guide RNA to induce indel mutations in the *Th* gene (sg*Th*) (Hunker et al., 2020). This AAV vector (or sgCTRL) was infused together with AAV-DIO-ChR2:mCherry into VTA of VGLUT2:Cre mice (Figure 4A). Immunohistochemical analysis showed 19% of Cas9-expressing (VGLUT2) VTA neurons expressed TH in the sgCTRL group, but only 2% expressed TH in the sg*Th* group (Figure 4B). Using *ex vivo* FSCV, we found substantially reduced ChR2-evoked DA release in the sg*Th*- compared to sgCTRL-injected brains, demonstrating successful disruption of DA release from VTA glutamate neurons (Figures 4C and 4D). Exogenous DA application rescued evoked DA transients from the sg*Th* brains, confirming that VTA glutamate terminals retained the ability to recycle and release DA when substrate was available (Figure 4E).

The sgCTRL and sg*Th* animals were also tested for self-stimulation of VTA glutamate neurons using the 2-hole ICSS task. In accordance with our results obtained in cKO mice, sgCTRL and sg*Th* mice displayed an equivalent preference for the nosepoke hole coupled to optogenetic stimulation of VTA glutamate terminals in NAc and switched preference when we switched the active nosepoke (Figure 4F). We observed similar results when the active nosepoke hole was coupled to optogenetic

Please cite this article in press as: Zell et al., VTA Glutamate Neuron Activity Drives Positive Reinforcement Absent Dopamine Co-release, Neuron (2020), https://doi.org/10.1016/j.neuron.2020.06.011

CellPress

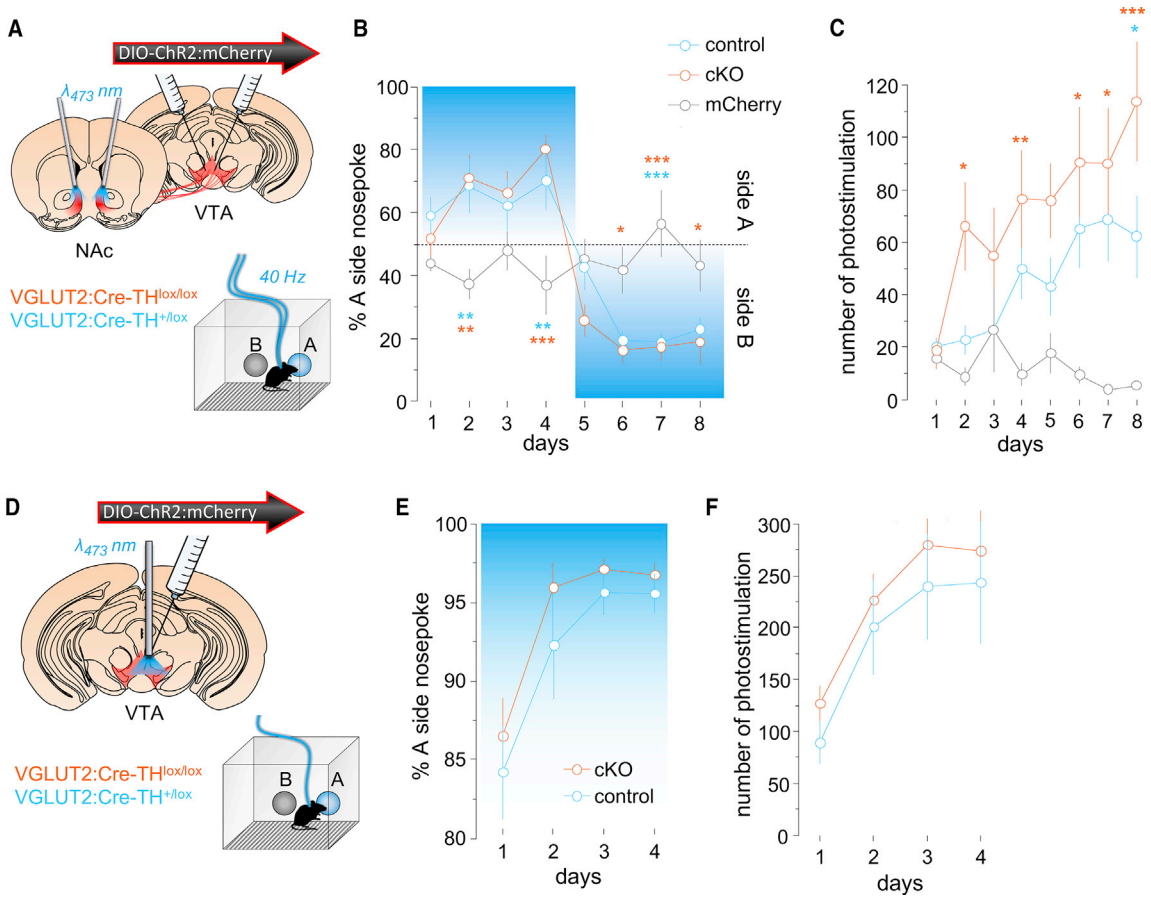

Figure 2. Self-stimulation of VTA Glutamate Neurons in cKO Mice

(A) Approach for self-stimulation of VTA glutamate terminals in NAc.

(B) ChR2:mCherry-expressing control and cKO mice displayed equivalent preference for the active nosepoke hole (days 1–4, hole A) and followed the active side after a switch (days 5–8, hole B); RM two-way ANOVA, main effect of day, $F(7, 175) = 18.6$, $p < 0.0001$ and interaction, $F(14,175) = 7.2$, $p < 0.0001$ (n = 10 control, n = 10 cKO, n = 8 mCherry). Tukey-Kramer's multiple comparisons test ***p < 0.001, **p < 0.01, *p < 0.05.

(C) ChR2:mCherry-expressing control and cKO increase the number of photostimulations earned across sessions compared to mCherry-expressing mice; RM two-way ANOVA, main effect of genotype, $F(2, 25) = 5.2$, $p = 0.013$ and interaction, $F(14, 175) = 1.8$, $p = 0.043$. Sidak's multiple comparisons test ***p < 0.001, **p < 0.01, *p < 0.05.

(D) Approach for self-stimulation of VTA glutamate cell bodies.

(E) Control and cKO mice developed an equivalent preference for the active nosepoke hole; RM two-way ANOVA, main effect of day, $F(3,57) = 15.9$, $p < 0.0001$.

(F) Control and cKO mice earned an equivalent number of photostimulations per session across days; RM two-way ANOVA, main effect of day, $F(3,57) = 27.2$, $p < 0.0001$ (n = 11 control, n = 10 cKO mice).

Data are represented as mean ± SEM. See also Figure S4.

stimulation of glutamate cell bodies in VTA (Figure 4G). These data provide additional independent evidence that VTA glutamate neuron activity can support positive reinforcement absent concomitant increases in DA signaling.

DISCUSSION

Prior work has demonstrated that, like VTA DA neurons, optogenetic activation of VTA glutamate neurons can support approach behaviors (Wang et al., 2015; Yoo et al., 2016). However, the extent to which VTA glutamate neurons rely on DA signaling to drive reward behaviors remained unclear. Indeed, a subset of VTA glutamate neurons co-express DA markers and co-release DA directly (Kawano et al., 2006; Lavin et al., 2005; Mingote et al., 2019; Stuber et al., 2010). In addition, VTA glutamate neurons make local synapses onto VTA DA neurons, representing another mechanism by which they might elicit increased DA signaling (Dobi et al., 2010; Qi et al., 2016; Yoo et al., 2016). In this report, we used conditional ablation of TH in glutamate neurons to test the contribution of DA transmission for reinforcement behaviors evoked by VTA glutamate neuron activity. We found that, while VTA glutamate neuron stimulation evokes DA release, this DA signal was not necessary for the activation of VTA glutamate neurons to support self-stimulation and approach behaviors. We thus propose that glutamate and DA projections from VTA to NAc represent partially overlapping but functionally distinct parallel pathways that can independently and distinctively support positive reinforcement.

Please cite this article in press as: Zell et al., VTA Glutamate Neuron Activity Drives Positive Reinforcement Absent Dopamine Co-release, Neuron (2020), https://doi.org/10.1016/j.neuron.2020.06.011

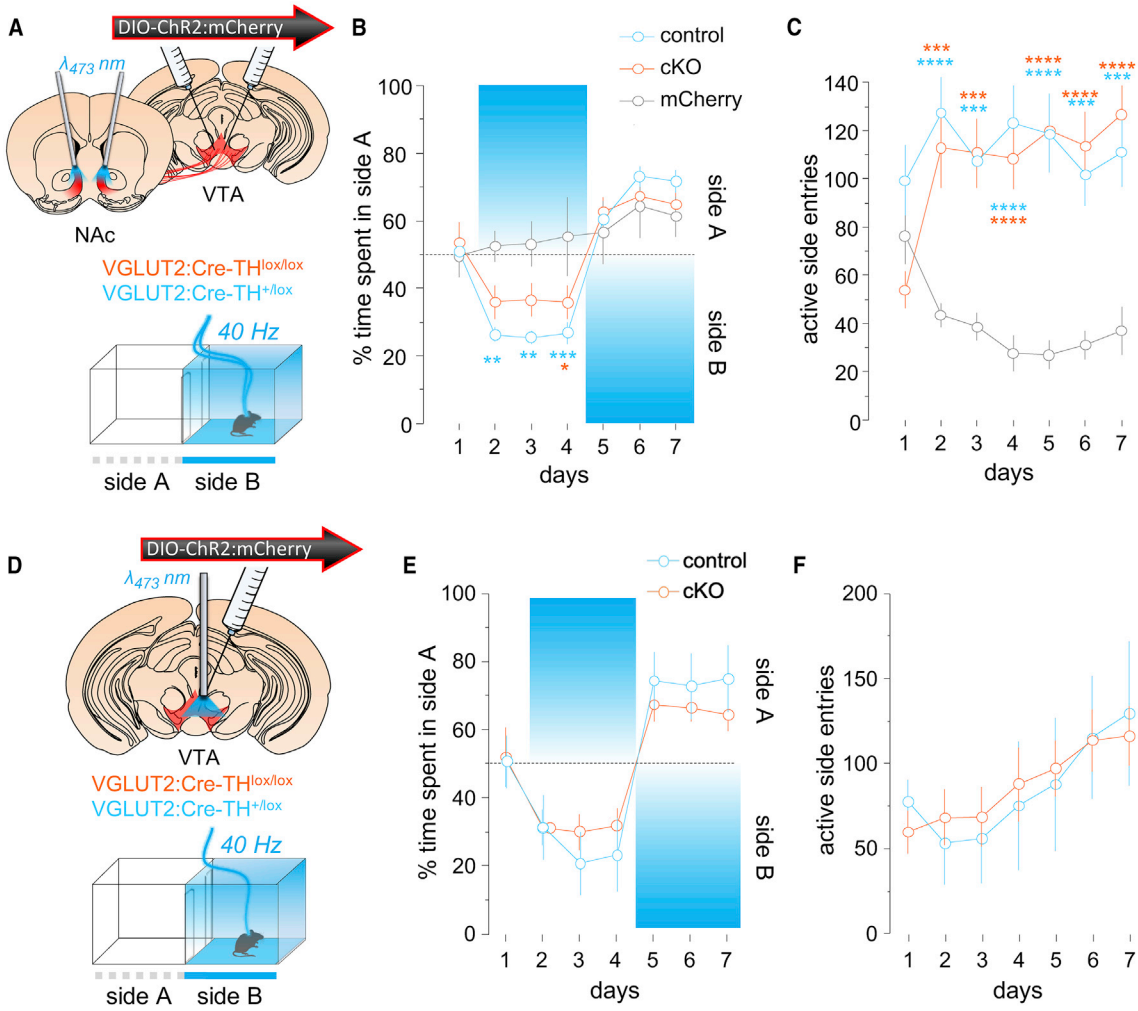

Figure 3. Behavior in Real-Time Place Preference Assay Is Unchanged by the Loss of DA Co-release in cKO Mice

(A) Schematic of the real-time place preference assay (RTPP) with stimulation of VTA glutamate terminals in NAc.

(B) ChR2:mCherry-expressing control and cKO mice spent less time in the active side compared to mCherry-expressing mice; RM two-way ANOVA, main effect of day, $F_{(6, 150)} = 23.8$, $p < 0.0001$ and interaction, $F_{(12,150)} = 3.7$, $p < 0.0001$ (n = 10 control mice, n = 10 cKO, n = 8 mCherry). Tukey-Kramer's multiple comparisons test ***p < 0.001, **p < 0.01, *p < 0.05.

(C) ChR2:mCherry-expressing control and cKO displayed an increase in approach rate into the active compartment; RM two-way ANOVA, main effect of genotype, $F_{(2, 25)} = 17.1$, $p < 0.0001$ and interaction $F_{(25,150)} = 7.3$, $p < 0.0001$. Tukey-Kramer's multiple comparisons test ****p < 0.0001, ***p < 0.001.

(D) Schematic of RTPP with stimulation of VTA glutamate cell bodies.

(E) Control and cKO mice spent less time in the side paired with laser; RM two-way ANOVA, main effect of day, $F_{(6,78)} = 14.6$, $p < 0.0001$.

(F) Control and cKO displayed a concomitant increase in approach rate across sessions; RM two-way ANOVA, main effect of day, $F_{(6,78)} = 6.6$, $p < 0.0001$ (n = 11 control, n = 10 cKO mice). Data are represented as mean ± SEM. See also Figure S4.

We consistently found that 10%–20% of VTA neurons that express VGLUT2 in adult mouse VTA also co-express the DA marker TH. This is in line with other recent reports and demonstrates that there is a larger population of non-DA glutamate neurons concentrated in medial VTA of mice (Hnasko et al., 2012; Yamaguchi et al., 2015). We provide new evidence that both *in vivo* and *ex vivo* optogenetic stimulation of glutamate cell bodies in VTA or their terminals can directly drive DA release in the medial NAc. Dual TH/VGLUT2-expressing neurons were virtually absent in our cKO and sg*Th* animals, as was optogenetic-evoked DA release, demonstrating successful disruption of DA co-release from VTA glutamate neurons in our models. Importantly, our data also suggest that any DA release that might be evoked through feedforward mechanisms or through recycling of extracellular DA released by other neurons is abrogated in the cKO mice that lacked evoked DA release *in vivo*. Despite the loss of DA signals in our cKO and sg*Th* animals, optogenetic activation of VTA glutamate neurons supported reinforcement and approach behaviors in our ICSS and RTPP assays that were indistinguishable from mice with intact DA/glutamate co-transmission. Similar results were obtained whether optogenetic stimulation was delivered at the level of VTA glutamate cell

Please cite this article in press as: Zell et al., VTA Glutamate Neuron Activity Drives Positive Reinforcement Absent Dopamine Co-release, Neuron (2020), https://doi.org/10.1016/j.neuron.2020.06.011

CellPress

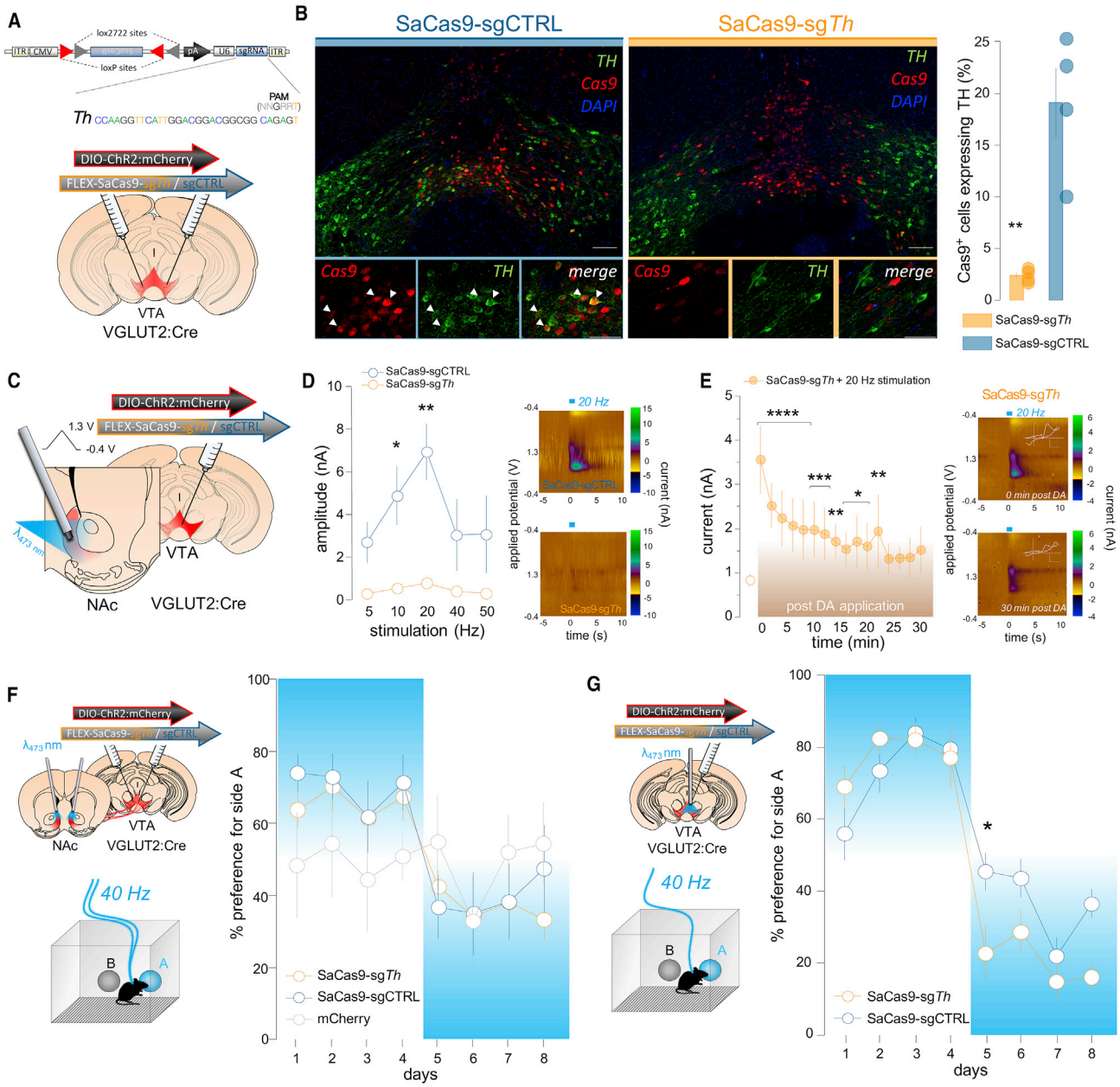

Figure 4. Self-stimulation of VTA Glutamate Terminals in NAc following CRISPR/Cas9 Disruption of TH and DA Co-release

(A) Schematic of AAV vectors and approach for CRISPR/Cas9 conditional deletion of *Th* from VTA glutamate neurons with ChR2:mCherry expression.

(B) Coronal sections show co-localization of TH in Cas9-expressing neurons in sgCTRL mice is absent in sg*Th* mice; scale, 100 μm (top), 50 μm (bottom); t test, **p = 0.0025 (n = 4 mice).

(C) Schematic of *ex vivo* FSCV approach.

(D) Photostimulation evoked DA transients from VTA glutamate terminals in medial NAc shell of sgCTRL but not sg*Th* mice; RM two-way ANOVA, main effect of frequency, $F_{(4, 24)} = 12.9$, $p < 0.0001$; treatment $F_{(1, 6)} = 7.1$, $p = 0.038$ and interaction, $F_{(4,24)} = 8.1$, $p = 0.0003$, Sidak's multiple comparisons test **p < 0.01, *p < 0.05 (n = 4 mice per group). Right insets show example color plots following 20 Hz photostimulation.

(E) Time course of opto-triggered DA transient sizes after bath application/wash; RM one-way ANOVA, main effect of treatment, $F_{(16, 48)} = 15.5$, $p < 0.0001$. Bonferroni's multiple comparisons test ****p < 0.0001, ***p < 0.001, **p < 0.01, *p < 0.05 (n = 4 mice). Right insets show example color plots following 20 Hz photostimulation at 0 min (top) and 30 min (bottom) after DA bath application/wash. Voltammogram scale: 2 nA; 0.4 V.

(F) Left: approach for self-stimulation of VTA glutamate terminals in NAc. Right: mice injected with either sg*Th* or sgCTRL develop an equivalent preference for the active nosepoke hole; RM two-way ANOVA, main effect of day, $F_{(7,126)} = 5.7$, $p < 0.0001$ (n = 7 sg*Th*, n = 8 sgCTRL, n = 6 mCherry mice).

(legend continued on next page)

Please cite this article in press as: Zell et al., VTA Glutamate Neuron Activity Drives Positive Reinforcement Absent Dopamine Co-release, Neuron (2020), https://doi.org/10.1016/j.neuron.2020.06.011

bodies, or their terminals in NAc. Thus, a concomitant increase in DA signaling does not appear necessary for behavioral reinforcement driven by VTA glutamate neuron activity.

Consistent with our previous observations, we found that the same animals that readily self-stimulated VTA glutamate neurons displayed counter-intuitive avoidance behavior in the RTPP assay (Yoo et al., 2016). However, the reduction in time spent in the active chamber was accompanied by an increased approach rate to that same active chamber, and both of these findings were also observed in the cKO. This pattern of behavior increases the number of short duration stimuli and probably reflects mice adjusting their behavior over time to optimize their preferred pattern of stimulation. Indeed, using an instrumental assay, mice displayed strong preference for brief stimulation of VTA glutamate neurons, and by comparison longer stimulation of VTA DA neurons was preferred (Yoo et al., 2016). We therefore hypothesize that both VTA DA and glutamate neuron activity can drive positive reinforcement but that they do so in distinctive ways and that reward driven by VTA glutamate neuron activity does not depend on accompanying increases in DA release.

An alternative hypothesis is that different subpopulations of VTA glutamate neurons differentially drive reward and aversion through different mechanisms, similar to different projection-defined VTA DA sub-populations (de Jong et al., 2019). Indeed, initial investigations of VTA glutamate neuron activity *in vivo* shows a diversity of responses to salient rewarding and aversive stimuli (Montardy et al., 2019; Root et al., 2018b). Thus, one population of VTA glutamate neurons could drive approach through intra-VTA excitation of DA neurons, while another population may drive avoidance via projections to NAc or other distal structures. In this case, perhaps different patterns of stimulation differentially recruit subpopulations of VTA glutamate neurons resulting in complex sequences of approach and avoidance. However, our present findings argue against this mechanism, as mice that lack DA release evoked by VTA glutamate neuron stimulation continue to self-stimulate VTA glutamate cell bodies or terminals in NAc. Further, our finding that mice that self-stimulate in an operant assay can show apparent place avoidance in the RTPP assay caution against interpreting widely used measures of avoidance behaviors as conclusively indicative of aversion. Instead, we suggest that a reduced approach rate or evidence of a negative affective reaction (e.g., conditioned avoidance or innate fear responses) might be necessary to conclude a stimulus is aversive. In any case, future studies will be necessary to reconcile the heterogeneity in VTA glutamate responses found *in vivo* with their functional roles in reward-related or other behaviors.

We also examined the impact of ablated DA synthesis and release from VTA VGLUT2 neurons on glutamate neurotransmission in the NAc using electrophysiology. Light-triggered DNQX-sensitive oEPSCs were recorded in both control and cKO mice, with no difference in their characteristics. However, we observed a significant reduction in paired-pulse depression in the cKO. This might indicate a lower release probability in the cKO, reduced D2-autoreceptor inhibition, or reduced glutamate quantal content as a consequence of reduced vesicular synergy (Adrover et al., 2014; Aguilar et al., 2017; Hnasko and Edwards, 2012; Hnasko et al., 2010; Silm et al., 2019).

Previous studies showed that VTA glutamate synapses might preferentially impact striatal interneurons (Cai and Ford, 2018; Chuhma et al., 2014, 2018; Qi et al., 2016). However, VTA glutamate neurons also directly synapse onto and can alter *in vivo* firing rate of NAc projection neurons (Mingote et al., 2015; Stuber et al., 2010; Tecuapetla et al., 2010; Wang et al., 2017). Yet it had not been determined whether D1 or D2 neurons, which play different functional roles, might be differentially connected to glutamate neurons from VTA. Although more studies will be necessary to assess how VTA inputs onto distinct NAc cell types influence their activity and effect on behavior *in vivo*, our data comparing oEPSC properties suggest no clear bias in the connectivity of VTA glutamate synapses on to MSN cell type.

Previous attempts at understanding the relative contributions of dual DA/glutamate co-transmission focused primarily on isolating the DA component. Mingote and colleagues achieved a partial reduction in glutamate release from midbrain DA neurons with intact DA transmission and observed a decrease in amphetamine sensitization and a potentiation of latent inhibition, implying a role for glutamate co-release in motivational salience and context discrimination (Mingote et al., 2017). Conditional deletion of VGLUT2 from DAT-expressing DA neurons abolished evoked oEPSCs in NAc and other terminal structures (Soden et al., 2016; Stuber et al., 2010; Tritsch et al., 2012) and led to reduced psychostimulant-induced locomotor activity and reward-seeking behaviors (Alsiö et al., 2011; Birgner et al., 2010; Hnasko et al., 2010; Wallén-Mackenzie et al., 2010), while self-stimulation of DA neurons was unaffected (Wang et al., 2017). Loss of VGLUT2 also sensitized DA neurons to neurotoxins, suggesting a role for VGLUT2 in selective DA neuron vulnerability (Shen et al., 2018; Steinkellner et al., 2018).

Here, we report the first results that isolate the glutamate component of VTA projection neurons using conditional genetic manipulations. We found that optogenetic stimulation of VTA glutamate neurons is sufficient to drive positive reinforcement and that this appears to be independent of concurrent DA release. Glutamate neurons therefore represent an alternate VTA pathway with unique features by which mesolimbic projections could integrate reward and motivational signals to control reward-seeking behaviors.

STAR★METHODS

Detailed methods are provided in the online version of this paper and include the following:

- KEY RESOURCES TABLE
- RESOURCE AVAILABILITY

(G) Left: approach for self-stimulation of VTA glutamate cell bodies. Right: mice injected with either sg*Th* or sgCTRL develop an equivalent preference for the active nosepoke hole; RM two-way ANOVA, main effect of day, $F_{(7, 84)} = 43.1$, $p < 0.0001$ and interaction, $F_{(7, 84)} = 2.7$, $p = 0.015$ (n = 6 sg*Th*, n = 8 sgCTRL mice). Sidak's multiple comparisons test *$p < 0.05$.
Data are represented as mean ± SEM. See also Figure S4.

SUPPLEMENTAL INFORMATION

Supplemental Information can be found online at https://doi.org/10.1016/j.neuron.2020.06.011.

ACKNOWLEDGMENTS

We thank Dr. Martin Darvas for providing TH floxed mice and Dr. Nicholas Spitzer for guidance on combining RNAscope with immunohistochemistry. This work has been supported by the NIH (R01DA036612, K99AG059834, K99MH119312, and K99DA046514), VA (I01 BX003759), a NIDA-INSERM postdoctoral Drug Abuse Research Fellowship, a Schrödinger postdoctoral fellowship from the Austrian Science Fund (J3656-B24), and a Jonas Salk Fellowship.

AUTHOR CONTRIBUTIONS

V.Z. and T.S.H. conceived the project and designed experiments. N.G.H. conducted and analyzed the *in vivo* FSCV recordings with support from X.J. V.Z. conducted and analyzed the electrophysiological recordings. V.Z. conducted and analyzed the behavioral and optogenetic studies with the help of E.S., L.F., and S.W. V.Z. conducted and analyzed *ex vivo* FSCV recordings with support from N.G.H. T.S. conducted and analyzed ISH/IHC experiments and behavioral pharmacology. A.C.H. and L.Z. provided AAV CRISPR/Cas9 constructs. V.Z. and T.S.H. supervised all aspects of the work. V.Z. and T.S.H. wrote the paper with editorial input from all authors.

DECLARATION OF INTERESTS

The authors declare no competing interests.

Received: February 11, 2019
Revised: April 21, 2020
Accepted: June 7, 2020
Published: June 30, 2020

REFERENCES

Adrover, M.F., Shin, J.H., and Alvarez, V.A. (2014). Glutamate and dopamine transmission from midbrain dopamine neurons share similar release properties but are differentially affected by cocaine. J. Neurosci. *34*, 3183–3192.

Aguilar, J.I., Dunn, M., Mingote, S., Karam, C.S., Farino, Z.J., Sonders, M.S., Choi, S.J., Grygoruk, A., Zhang, Y., Cela, C., et al. (2017). Neuronal Depolarization Drives Increased Dopamine Synaptic Vesicle Loading via VGLUT. Neuron *95*, 1074–1088.

Alsiö, J., Nordenankar, K., Arvidsson, E., Birgner, C., Mahmoudi, S., Halbout, B., Smith, C., Fortin, G.M., Olson, L., Descarries, L., et al. (2011). Enhanced sucrose and cocaine self-administration and cue-induced drug seeking after loss of VGLUT2 in midbrain dopamine neurons in mice. J. Neurosci. *31*, 12593–12603.

Bariselli, S., Glangetas, C., Tzanoulinou, S., and Bellone, C. (2016). Ventral tegmental area subcircuits process rewarding and aversive experiences. J. Neurochem. *139*, 1071–1080.

Berridge, K.C., Robinson, T.E., and Aldridge, J.W. (2009). Dissecting components of reward: 'liking', 'wanting', and learning. Curr. Opin. Pharmacol. *9*, 65–73.

Bérubé-Carrière, N., Riad, M., Dal Bo, G., Lévesque, D., Trudeau, L.É., and Descarries, L. (2009). The dual dopamine-glutamate phenotype of growing mesencephalic neurons regresses in mature rat brain. J. Comp. Neurol. *517*, 873–891.

Birgner, C., Nordenankar, K., Lundblad, M., Mendez, J.A., Smith, C., le Grevès, M., Galter, D., Olson, L., Fredriksson, A., Trudeau, L.E., et al. (2010). VGLUT2 in dopamine neurons is required for psychostimulant-induced behavioral activation. Proc. Natl. Acad. Sci. USA *107*, 389–394.

Cai, Y., and Ford, C.P. (2018). Dopamine Cells Differentially Regulate Striatal Cholinergic Transmission across Regions through Corelease of Dopamine and Glutamate. Cell Rep. *25*, 3148–3157.

Chuhma, N., Choi, W.Y., Mingote, S., and Rayport, S. (2009). Dopamine neuron glutamate cotransmission: frequency-dependent modulation in the mesoventromedial projection. Neuroscience *164*, 1068–1083.

Chuhma, N., Mingote, S., Moore, H., and Rayport, S. (2014). Dopamine neurons control striatal cholinergic neurons via regionally heterogeneous dopamine and glutamate signaling. Neuron *81*, 901–912.

Chuhma, N., Mingote, S., Yetnikoff, L., Kalmbach, A., Ma, T., Ztaou, S., Sienna, A.C., Tepler, S., Poulin, J.F., Ansorge, M., et al. (2018). Dopamine neuron glutamate cotransmission evokes a delayed excitation in lateral dorsal striatal cholinergic interneurons. eLife 7. Published online October 8, 2018. https://doi.org/10.7554/eLife.39786.

Clark, J.J., Sandberg, S.G., Wanat, M.J., Gan, J.O., Horne, E.A., Hart, A.S., Akers, C.A., Parker, J.G., Willuhn, I., Martinez, V., et al. (2010). Chronic microsensors for longitudinal, subsecond dopamine detection in behaving animals. Nat. Methods *7*, 126–129.

Cole, S.L., Robinson, M.J.F., and Berridge, K.C. (2018). Optogenetic self-stimulation in the nucleus accumbens: D1 reward versus D2 ambivalence. PLoS ONE *13*, e0207694.

Darvas, M., and Palmiter, R.D. (2010). Restricting dopaminergic signaling to either dorsolateral or medial striatum facilitates cognition. J. Neurosci. *30*, 1158–1165.

de Jong, J.W., Afjei, S.A., Pollak Dorocic, I., Peck, J.R., Liu, C., Kim, C.K., Tian, L., Deisseroth, K., and Lammel, S. (2019). A Neural Circuit Mechanism for Encoding Aversive Stimuli in the Mesolimbic Dopamine System. Neuron *101*, 133–151.

Dobi, A., Margolis, E.B., Wang, H.-L., Harvey, B.K., and Morales, M. (2010). Glutamatergic and nonglutamatergic neurons of the ventral tegmental area establish local synaptic contacts with dopaminergic and nondopaminergic neurons. J. Neurosci. *30*, 218–229.

Fields, H.L., Hjelmstad, G.O., Margolis, E.B., and Nicola, S.M. (2007). Ventral tegmental area neurons in learned appetitive behavior and positive reinforcement. Annu. Rev. Neurosci. *30*, 289–316.

Heien, M.L.A.V., Khan, A.S., Ariansen, J.L., Cheer, J.F., Phillips, P.E.M., Wassum, K.M., and Wightman, R.M. (2005). Real-time measurement of dopamine fluctuations after cocaine in the brain of behaving rats. Proc. Natl. Acad. Sci. USA *102*, 10023–10028.

Heusner, C.L., Beutler, L.R., Houser, C.R., and Palmiter, R.D. (2008). Deletion of GAD67 in dopamine receptor-1 expressing cells causes specific motor deficits. Genesis *46*, 357–367.

Hnasko, T.S., and Edwards, R.H. (2012). Neurotransmitter corelease: mechanism and physiological role. Annu. Rev. Physiol. *74*, 225–243.

Hnasko, T.S., Chuhma, N., Zhang, H., Goh, G.Y., Sulzer, D., Palmiter, R.D., Rayport, S., and Edwards, R.H. (2010). Vesicular glutamate transport promotes dopamine storage and glutamate corelease in vivo. Neuron *65*, 643–656.

Hnasko, T.S., Hjelmstad, G.O., Fields, H.L., and Edwards, R.H. (2012). Ventral tegmental area glutamate neurons: electrophysiological properties and projections. J. Neurosci. *32*, 15076–15085.

Howard, C.D., Li, H., Geddes, C.E., and Jin, X. (2017). Dynamic Nigrostriatal Dopamine Biases Action Selection. Neuron *93*, 1436–1450.

Hunker, A.C., Soden, M.E., Krayushkina, D., Heymann, G., Awatramani, R., and Zweifel, L.S. (2020). Conditional Single Vector CRISPR/SaCas9 Viruses for Efficient Mutagenesis in the Adult Mouse Nervous System. Cell Rep. *30*, 4303–4316.

Ikemoto, S., and Bonci, A. (2014). Neurocircuitry of drug reward. Neuropharmacology *76* (Pt B), 329–341.

Kawano, M., Kawasaki, A., Sakata-Haga, H., Fukui, Y., Kawano, H., Nogami, H., and Hisano, S. (2006). Particular subpopulations of midbrain and hypothalamic dopamine neurons express vesicular glutamate transporter 2 in the rat brain. J. Comp. Neurol. *498*, 581–592.

Keiflin, R., and Janak, P.H. (2015). Dopamine Prediction Errors in Reward Learning and Addiction: From Theory to Neural Circuitry. Neuron *88*, 247–263.

Keithley, R.B., and Wightman, R.M. (2011). Assessing principal component regression prediction of neurochemicals detected with fast-scan cyclic voltammetry. ACS Chem. Neurosci. *2*, 514–525.

Keithley, R.B., Heien, M.L., and Wightman, R.M. (2009). Multivariate concentration determination using principal component regression with residual analysis. Trends Analyt. Chem. *28*, 1127–1136.

Kouwenhoven, W.M., Fortin, G., Penttinen, A.-M., Florence, C., Delignat-Lavaud, B., Bourque, M.-J., Trimbuch, T., Luppi, M.P., Poulin, J.-F., Rosenmund, C., et al. (2019). Vglut2 expression in dopamine neurons contributes to post-lesional striatal reinnervation. bioRxiv, 12.23.887323.

Kravitz, A.V., Tye, L.D., and Kreitzer, A.C. (2012). Distinct roles for direct and indirect pathway striatal neurons in reinforcement. Nat. Neurosci. *15*, 816–818.

Lavin, A., Nogueira, L., Lapish, C.C., Wightman, R.M., Phillips, P.E., and Seamans, J.K. (2005). Mesocortical dopamine neurons operate in distinct temporal domains using multimodal signaling. J. Neurosci. *25*, 5013–5023.

Lein, E.S., Hawrylycz, M.J., Ao, N., Ayres, M., Bensinger, A., Bernard, A., Boe, A.F., Boguski, M.S., Brockway, K.S., Byrnes, E.J., et al. (2007). Genome-wide atlas of gene expression in the adult mouse brain. Nature *445*, 168–176.

Lobo, M.K., and Nestler, E.J. (2011). The striatal balancing act in drug addiction: distinct roles of direct and indirect pathway medium spiny neurons. Front. Neuroanat. *5*, 41.

Mendez, J.A., Bourque, M.-J., Dal Bo, G., Bourdeau, M.L., Danik, M., Williams, S., Lacaille, J.-C., and Trudeau, L.-E. (2008). Developmental and target-dependent regulation of vesicular glutamate transporter expression by dopamine neurons. J. Neurosci. *28*, 6309–6318.

Mingote, S., Chuhma, N., Kusnoor, S.V., Field, B., Deutch, A.Y., and Rayport, S. (2015). Functional Connectome Analysis of Dopamine Neuron Glutamatergic Connections in Forebrain Regions. J. Neurosci. *35*, 16259–16271.

Mingote, S., Chuhma, N., Kalmbach, A., Thomsen, G.M., Wang, Y., Mihali, A., Sferrazza, C., Zucker-Scharff, I., Siena, A.C., Welch, M.G., et al. (2017). Dopamine neuron dependent behaviors mediated by glutamate cotransmission. eLife *6*. Published online July 13, 2017. https://doi.org/10.7554/eLife.27566.

Mingote, S., Amsellem, A., Kempf, A., Rayport, S., and Chuhma, N. (2019). Dopamine-glutamate neuron projections to the nucleus accumbens medial shell and behavioral switching. Neurochem. Int. *129*, 104482.

Montardy, Q., Zhou, Z., Lei, Z., Liu, X., Zeng, P., Chen, C., Liu, Y., Sanz-Leon, P., Huang, K., and Wang, L. (2019). Characterization of glutamatergic VTA neural population responses to aversive and rewarding conditioning in freely-moving mice. Sci. Bull. (Beijing) *64*, 1167–1178.

Pupe, S., and Wallén-Mackenzie, Å. (2015). Cre-driven optogenetics in the heterogeneous genetic panorama of the VTA. Trends Neurosci. *38*, 375–386.

Qi, J., Zhang, S., Wang, H.L., Barker, D.J., Miranda-Barrientos, J., and Morales, M. (2016). VTA glutamatergic inputs to nucleus accumbens drive aversion by acting on GABAergic interneurons. Nat. Neurosci. *19*, 725–733.

Root, D.H., Zhang, S., Barker, D.J., Miranda-Barrientos, J., Liu, B., Wang, H.-L., and Morales, M. (2018a). Selective Brain Distribution and Distinctive Synaptic Architecture of Dual Glutamatergic-GABAergic Neurons. Cell Rep. *23*, 3465–3479.

Root, D.H., Estrin, D.J., and Morales, M. (2018b). Aversion or Salience Signaling by Ventral Tegmental Area Glutamate Neurons. iScience *2*, 51–62.

Shen, H., Marino, R.A.M., McDevitt, R.A., Bi, G.-H., Chen, K., Madeo, G., Lee, P.-T., Liang, Y., De Biase, L.M., Su, T.-P., et al. (2018). Genetic deletion of vesicular glutamate transporter in dopamine neurons increases vulnerability to MPTP-induced neurotoxicity in mice. Proc. Natl. Acad. Sci. USA *115*, E11532–E11541.

Silm, K., Yang, J., Marcott, P.F., Asensio, C.S., Eriksen, J., Guthrie, D.A., Newman, A.H., Ford, C.P., and Edwards, R.H. (2019). Synaptic Vesicle Recycling Pathway Determines Neurotransmitter Content and Release Properties. Neuron *102*, 786–800.

Soden, M.E., Miller, S.M., Burgeno, L.M., Phillips, P.E.M., Hnasko, T.S., and Zweifel, L.S. (2016). Genetic Isolation of Hypothalamic Neurons that Regulate Context-Specific Male Social Behavior. Cell Rep. *16*, 304–313.

Steinkellner, T., Zell, V., Farino, Z.J., Sonders, M.S., Villeneuve, M., Freyberg, R.J., Przedborski, S., Lu, W., Freyberg, Z., and Hnasko, T.S. (2018). Role for VGLUT2 in selective vulnerability of midbrain dopamine neurons. J. Clin. Invest. *128*, 774–788.

Stuber, G.D., Hnasko, T.S., Britt, J.P., Edwards, R.H., and Bonci, A. (2010). Dopaminergic terminals in the nucleus accumbens but not the dorsal striatum corelease glutamate. J. Neurosci. *30*, 8229–8233.

Tecuapetla, F., Patel, J.C., Xenias, H., English, D., Tadros, I., Shah, F., Berlin, J., Deisseroth, K., Rice, M.E., Tepper, J.M., and Koos, T. (2010). Glutamatergic signaling by mesolimbic dopamine neurons in the nucleus accumbens. J. Neurosci. *30*, 7105–7110.

Thibeault, K.C., Kutlu, M.G., Sanders, C., and Calipari, E.S. (2019). Cell-type and projection-specific dopaminergic encoding of aversive stimuli in addiction. Brain Res. *1713*, 1–15.

Tritsch, N.X., Ding, J.B., and Sabatini, B.L. (2012). Dopaminergic neurons inhibit striatal output through non-canonical release of GABA. Nature *490*, 262–266.

Trudeau, L.E., Hnasko, T.S., Wallén-Mackenzie, A., Morales, M., Rayport, S., and Sulzer, D. (2014). The multilingual nature of dopamine neurons. Prog. Brain Res. *211*, 141–164.

Wallén-Mackenzie, A., Wootz, H., and Englund, H. (2010). Genetic inactivation of the vesicular glutamate transporter 2 (VGLUT2) in the mouse: what have we learnt about functional glutamatergic neurotransmission? Ups. J. Med. Sci. *115*, 11–20.

Wang, H.L., Qi, J., Zhang, S., Wang, H., and Morales, M. (2015). Rewarding effects of optical stimulation of ventral tegmental area glutamatergic neurons. J. Neurosci. *35*, 15948–15954.

Wang, D.V., Viereckel, T., Zell, V., Konradsson-Geuken, Å., Broker, C.J., Talishinsky, A., Yoo, J.H., Galinato, M.H., Arvidsson, E., Kesner, A.J., et al. (2017). Disrupting Glutamate Co-transmission Does Not Affect Acquisition of Conditioned Behavior Reinforced by Dopamine Neuron Activation. Cell Rep. *18*, 2584–2591.

Yamaguchi, T., Wang, H.-L., Li, X., Ng, T.H., and Morales, M. (2011). Mesocorticolimbic glutamatergic pathway. J. Neurosci. *31*, 8476–8490.

Yamaguchi, T., Qi, J., Wang, H.L., Zhang, S., and Morales, M. (2015). Glutamatergic and dopaminergic neurons in the mouse ventral tegmental area. Eur. J. Neurosci. *41*, 760–772.

Yoo, J.H., Zell, V., Gutierrez-Reed, N., Wu, J., Ressler, R., Shenasa, M.A., Johnson, A.B., Fife, K.H., Faget, L., and Hnasko, T.S. (2016). Ventral tegmental area glutamate neurons co-release GABA and promote positive reinforcement. Nat. Commun. *7*, 13697.

Please cite this article in press as: Zell et al., VTA Glutamate Neuron Activity Drives Positive Reinforcement Absent Dopamine Co-release, Neuron (2020), https://doi.org/10.1016/j.neuron.2020.06.011

CellPress

STAR★METHODS

KEY RESOURCES TABLE

REAGENT or RESOURCE	SOURCE	IDENTIFIER
Antibodies		
Sheep Anti-tyrosine hydroxylase (TH)	Pel-Freeze	P60101-0
Rabbit Anti-tyrosine hydroxylase (TH)	Millipore	AB152
Rat Anti-dopamine transporter (DAT)	Millipore	MAB369
Rabbit Anti-DsRed	Clontech	632496
Rabbit Anti-HA	Sigma	H6908
Donkey Anti-Sheep Alexa Fluor 647	Jackson Immuno Research	713-605-147
Donkey Anti-Rat Alexa Fluor 488-conjugated	Jackson Immuno Research	712-545-150
Donkey Anti-Rabbit Fluor 594-conjugated	Jackson Immuno Research	711-585-152
Donkey Anti-Rabbit Fluor 647-conjugated	Jackson Immuno Research	711-605-152
Bacterial and Virus Strains		
rAAV1-EF1α-DIO-hChR2(H134R)-mCherry	UNC virus vector core	N/A
rAAV5-EF1α-DIO-mCherry	UNC virus vector core	N/A
rAAV5-EF1a-DIO-hChR2(H134R)-EYFP	UNC virus vector core	N/A
AAV1-FLEX-SaCas9-sgTh	Hunker et al., 2020	N/A
Chemicals, Peptides, and Recombinant Proteins		
6,7-Dinitroquinoxaline-2,3(1H,4H)-dione (DNQX)	Sigma-Aldrich	D0540
Dopamine hydrochloride	Alfa Aesar	A11136
3,4-Dihydroxy-L-phenylalanine (L-DOPA)	Sigma-Aldrich	D9628
Benserazide hydrochloride	Sigma-Aldrich	B7283
D-amphetamine hemisulfate	Sigma-Aldrich	A5880
SKF81297 hydrobromide	Tocris	1447
Critical Commercial Assays		
RNAscope Multiplex Fluorescent Kit	Advanced Cell Diagnostics	320850
Mm-Slc17a6-C1 (VGLUT2 Antisense probe)	Advanced Cell Diagnostics	319171
Experimental Models: Organisms/Strains		
Mouse: Slc17a6$^{tm2(cre)Lowl}$	The Jackson Laboratory	016963
Mouse: Th$^{lox/lox}$	Darvas and Palmiter, 2010	N/A
Mouse: Tg(Adora2a-cre)K139Gsat/Mmcd	The Jackson Laboratory	036158
Mouse: Drd1a$^{+/Cr}$	Heusner et al., 2008	N/A

RESOURCE AVAILABILITY

Lead Contact

Further information and requests for resources and reagents should be directed to and will be fulfilled by the Lead Contact, Thomas S. Hnasko (thnasko@health.ucsd.edu)

Materials Availability

- This study did not generate new plasmids.
- This study did not generate new mouse lines.
- This study did not generate new unique reagents.

Data and Code Availability

- This study did not generate any code.
- This study did not generate any particular type of dataset.

Please cite this article in press as: Zell et al., VTA Glutamate Neuron Activity Drives Positive Reinforcement Absent Dopamine Co-release, Neuron (2020), https://doi.org/10.1016/j.neuron.2020.06.011

EXPERIMENTAL MODEL AND SUBJECT DETAILS

Animals

Mice were bred at the University of California, San Diego (UCSD), group housed (max 5 mice/cage), and maintained on a 12h light–dark cycle with food and water available *ad libitum* unless noted. Initial breeders for *Slc17a6*$^{tm2(cre)Lowl}$ and Tg(*Adora2a*-cre) K139Gsat/Mmcd breeders were obtained from The Jackson Laboratory (stock no: 016963 and 036158, respectively). *Drd1a*$^{+/Cre}$ (Heusner et al., 2008) breeders were obtained from the lab of Larry Zweifel (University of Washington) and *Th*$^{lox/lox}$ mice were provided by the lab of Martin Darvas (University of Washington). All mice were maintained fully backcrossed on to C57BL/6. Control and Th cKO mice were generated by breeding homozygous *Th*$^{lox/lox}$ mice to double heterozygous *Th*$^{+/lox}$; *Slc17a6*$^{+/Cre}$ mice and heterozygous littermates were used as controls. Drd1$^{+/Cre}$ or Adora2a-Cre mice were bred to *Slc17a6*$^{Cre/Cre}$. Mice were 3-8 months old for behavioral experiments, *in vivo* FSCV and immunohistochemistry and 8-12 weeks old for slice electrophysiology and *ex vivo* FSCV experiments. Male and female mice were included in all experiments, and all experiments performed in accordance with protocols approved by the UCSD Institutional Animal Care and Use Committee.

METHOD DETAILS

Stereotactic surgery

Mice (> 4-week-old) were anaesthetized with isoflurane, placed in a stereotaxic frame (Kopf), and 300 nL of AAV1-EF1α-DIO-ChR2(H134R):mCherry or AAV5-EF1α-DIO-mCherry (UNC gene therapy center virus vector core) infused into the VTA of heterozygote (*Th*$^{+/lox}$; *Slc17a6*$^{+/Cre}$) and TH cKO (*Th*$^{lox/lox}$; *Slc17a6*$^{+/Cre}$) mice (ml: ±0.35, ap: −3.4, dv: −4.4 mm relative to Bregma) at 100 nl.min^{-1} (WPI UltraMicroPump) using custom made 30-gauge stainless steel (Plastics One, VA) injectors. For CRISPR/Cas9 experiments VGLUT2:Cre mice were injected bilaterally with either AAV1-FLEX-SaCas9-U6-sg*Th* or a control vector targeting human *Th* at a region of low complementarity AAV1-FLEX-SaCas9-U6-sg*Th*(human) (sgCTRL) (Hunker et al., 2020). Cas9 vectors were mixed 2:1 with AAV1-EF1α-DIO-ChR2(H134R):mCherry and a total of 300 nL injected per side. For the electrophysiology recordings from defined D1 or D2 type neurons, *Drd1*$^{+/cre}$; *Slc17a6*$^{+/Cre}$ or *Adora2a-Cre; Slc17a6*$^{+/Cre}$ mice were infused with 2 different AAVs unilaterally: first with AAV5-EF1α-DIO-mCherry in the medial NAc shell (ml: −0.5, ap: +1.1, dv: −4.5) plus AAV5-EF1α-DIO-hChR2(H134R)-EYFP in VTA (ml: −0.35, ap: −3.4, dv: −4.4). For each infusion, the injection tip was left in place for 10 min and then slowly retracted. Mice used in behavioral experiments, were also implanted with a 200-μm-core optic fiber (Newdoon Inc.) inserted either unilaterally in VTA (ml: ±0.5, ap: −3.4, dv: −4.0) or bilaterally in NAc following a 10° mediolateral angle (ml: ± 1.13, ap: +1.4, dv: −3.81) following viral infusion. Fibers were stabilized using dental cement (Lang dental) secured by at least two skull screws. Animals were treated with the analgesic Carprofen (Pfizer, 5mg.kg^{-1} s.c.) before and after surgery. Mice were monitored daily and allowed to recover from surgery for > 3 weeks before subsequent assay.

Immunohistochemistry

Mice were deeply anaesthetized with pentobarbital (200 mg.kg^{-1} i.p.; Virbac) and transcardially perfused with 10–20 mL of phosphate-buffered saline (PBS) followed by 60-70 mL of 4% paraformaldehyde (PFA) at a rate of 6 ml.min^{-1}. Brains were extracted, post-fixed in 4% PFA at 4°C overnight and cryoprotected in 30% sucrose in PBS for 48–72h at 4°C. Brains were snap frozen in chilled isopentane and stored at −80°C. Sections (30 μm) were cut using a cryostat (CM3050S, Leica) and collected in PBS containing 0.01% sodium azide. For immunostaining, brain sections were blocked with 5% normal donkey serum in PBS containing 0.2% Triton X-100 (block) for 1 h at room temperature. Sections were then incubated with one or more of the following primary antibodies (rabbit anti-TH, 1:2,000, Millipore AB152; sheep anti-TH, 1:1,000, Pel-Freez P60101-0; rabbit anti-DsRed, 1:2000, Clontech 632496; rat anti-DAT 1:1000, Millipore MAB369; mouse anti-TH 1:1000, Millipore MAB318; rabbit anti-HA, 1:1000, H6908, Sigma - SaCas9 has a hemagglutinin (HA)-epitope tag on the C terminus) in blocking buffer overnight at 4°C. Sections were rinsed 3x15 min with PBS and incubated in appropriate secondary antibodies (Jackson ImmunoResearch) conjugated to Alexa 488, Alexa 594 or Alexa 647 fluorescent dyes (5 μg.ml^{-1}) for 2 h at room temperature. Sections were washed 3x15 min with PBS, mounted onto glass slides and coverslipped with Fluoromount-G mounting medium (Southern Biotech) + DAPI (Roche, 0.5 μg.ml^{-1}).

Images were acquired using widefield epifluorescence (Zeiss AxioObserver). For the colocalization of TH with mCherry, images of VTA were acquired using a 20X objective with identical acquisition settings across slides. For fluorescence densitometry, images of the ventral and dorsal striatum were acquired and four to six striatal sections were analyzed per animal. Briefly, regions of interest in the striatum were delineated and pixel densities were quantified using ImageJ. Background staining was quantified by measurement of pixel intensities in the corpus callosum and subtracted from striatal regions for normalization. For cell counting, sections covering the rostrocaudal extent of the VTA were collected and stained for TH and mCherry (Figure 1D) or HA (to visualize SaCas9) and TH (Figure 4B). Three to four sections covering the VTA were counted per animal by an experimenter blind to the treatment. For densitometry quantification, four striatal sections per animal were analyzed using ImageJ. Regions of interest in the dorsal and ventral striatum were delineated and pixel densities were quantified using ImageJ. Background staining was quantified by measurement of pixel density in the dorsomedial cortex and subtracted from striatal regions for normalization.

Please cite this article in press as: Zell et al., VTA Glutamate Neuron Activity Drives Positive Reinforcement Absent Dopamine Co-release, Neuron (2020), https://doi.org/10.1016/j.neuron.2020.06.011

In situ hybridization followed by immunohistochemistry

Mice were anesthetized with pentobarbital (200 mg.kg^{-1}, i.p.) and transcardially perfused with 4% PFA. Brains were removed, post-fixed in 4% PFA overnight, and cryoprotected in 30% sucrose in PBS for 48-72h. Brains were cut serially (16 μm) on a cryostat (CM3050S, Leica) and mounted directly onto Superfrost glass slides (Fisher). Sections were stored at –80°C before starting the RNA-scope assay (Advanced Cell Diagnostics). Briefly, slides were baked at 60°C for 30 min, rehydrated in PBS followed by boiling in Target Retrieval Solution (ACD) for 5 min. Slides were washed twice in distilled water and once in 100% ethanol before incubation with protease III (ACD) at 40°C for 30 min. RNA hybridization was performed according to the Fluorescent Multiplex Kit (ACD) using an antisense probe against *Slc17a6*/VGLUT2 (ACD 319171-C1). After the last wash step, slides were rinsed two times in PBS, blocked in 5% normal donkey serum/0.2% Triton X-100 in PBS for 1h at room temperature and incubated with primary antibodies (rabbit Anti-TH 1:500; AB152, Chemicon; rat-Anti-DAT 1:500; MAB369, Chemicon) overnight at 4°C in blocking buffer. Next day, slides were washed three times in PBS for 15 min and incubated with secondary antibodies (1:400; Alexa Fluor 488 and 647; Jackson ImmunoReseach) for two hours at room temperature. Finally, slides were washed three times in PBS for 15 min and coverslipped using DAPI-containing Fluoromount-G. Images were taken at 20x magnification using a Zeiss Axio Observer Epifluorescence microscope. For cell counting quantification, sections covering the rostrocaudal extent of the VTA were collected and stained for TH, DAT and VGLUT2. For RNAscope quantification of VGLUT2-positive neurons, cells were deemed positive above a threshold of 4 puncta. 3-4 sections covering the VTA were counted per animal by an experimenter blind to the treatment.

Electrophysiological recordings from adult brain slices

Adult mice (7–12 wks) were deeply anaesthetized with pentobarbital (100 mg.kg^{-1} i.p.; Virbac) and transcardially perfused with 10 mL ice-cold sucrose-artificial cerebrospinal fluid (ACSF) containing (in mM): 75 sucrose, 87 NaCl, 2.5 KCl, 7 $MgCl_2$, 0.5 $CaCl_2$, 1.25 NaH_2PO_4, 25 $NaHCO_3$ and continuously bubbled with carbogen (95% O_2–5% CO_2). Brains were extracted, and 200-mm coronal slices were cut in sucrose-ACSF using a Leica Vibratome (vt1200). Slices were transferred to a perfusion chamber containing ACSF at 31°C (in mM): 126 NaCl, 2.5 KCl, 1.2 $MgCl_2$, 2.4 $CaCl_2$, 1.4 NaH_2PO_4, 25 $NaHCO_3$, 11 glucose, continuously bubbled in carbogen. After > 45 min recovery, slices were transferred to a recording chamber continuously perfused with ACSF (2–3 ml.min^{-1}) maintained at 29–31°C using an in-line heater. Patch pipettes (3.5–5.5 MΩ) were pulled from borosilicate glass (King Precision Glass) and filled with internal recording solution containing (in mM): 120 $CsCH_3SO_3$, 20 HEPES, 0.4 EGTA, 2.8 NaCl, 5 TEA, 2.5 Mg-ATP, 0.25 Na-GTP, at pH 7.25 and 285 ± 5 mOsm. mCherry-labeled VGLUT2 VTA terminals as well as D1R- and A2a-expressing NAc neurons were visualized by epifluorescence and visually guided patch recordings were made using infrared-differential interference contrast (IR-DIC) illumination (Axiocam MRm, Examiner.A1, Zeiss). ChR2 was activated by flashing blue light (5-ms) through the light path of the microscope using a light-emitting diode (UHP-LED460, Prizmatix) under computer control. Excitatory postsynaptic currents (EPSCs) were recorded in whole-cell voltage clamp (Multiclamp 700B amplifier, Axon Instruments), filtered at 2 KHz, digitized at 10 KHz (Axon Digidata 1550, Axon Instruments), and collected online using pClamp 10 software (Molecular Device). Series resistance and capacitance were electronically compensated before recordings. Estimated liquid-junction potential was 12mV and left uncorrected. Series resistance and/or leak current were monitored during recordings and cells that showed > 25% change during recordings were considered unstable and discarded. Neurons were held in voltage-clamp at −60mV to record AMPAR EPSCs in whole-cell configuration and single-pulse (5-ms) photostimuli were applied every 55 s and 10 photo-evoked currents were averaged per neuron per condition. DMSO stock solution of DNQX (10 mM, Sigma) was diluted 1,000-fold in ACSF and bath applied at 10 μM. Current sizes were calculated by using peak amplitude from baseline. Decay time constants (τ) were calculated by fitting an exponential function to each averaged current trace using the following formula: $f(t) = e^{-t/\tau}+C$.

Fast-scan cyclic voltammetry recordings

In vivo FSCV

VGLUT2-Cre-expressing control and cKO mice were prepared as described above with Cre-dependent ChR2:mCherry virus infusion and optic fiber implantation targeting the VTA unilaterally. Following > 6 weeks recovery, mice were anesthetized with isoflurane (induced at 3%, maintained at 0.5%–1.5% throughout recordings) and placed in a stereotaxic frame (Kopf). A Ag/AgCl reference electrode was implanted in the contralateral hemisphere, and a carbon-fiber microelectrode (Clark et al., 2010) was lowered into the medial NAc shell (ml: ± 0.4, ap: 1.34, dv: −3.55 mm). A PC-based system running TarheelCV software written in LabView (National Instruments) was used for voltammetric waveform application and data acquisition. The potential at the carbon-fiber electrode was held at −0.4 V versus the Ag/AgCl reference, ramped to +1.3 V and back to −0.4 V at 400 V.s^{-1}. This voltammetric waveform initially was applied at 60 Hz for ~15 min and then at 10 Hz for the duration of the recording. Optogenetic stimulation was delivered to the VTA through the optic fiber coupled to a 473-nm laser (LaserGlow). Stimulation trains (1 s, 10 mW, 10 ms pulse width) at frequencies of 5, 10, 20, or 50 Hz were delivered every 2 min in interleaved, ascending order, with four repetitions of each frequency. This full stimulation protocol was repeated at 3-5 recording sites per animal 200 μm apart in the dorsoventral axis. This multisite procedure increased chances of appropriate recording site within the medial NAc shell, then confirmed using post hoc histology. The last recording site was marked with an electrolytic lesion (70 μA, 20 s). When multiple recording sites were located within the medial shell for a given animal, a single site was included in the final group analyses, based on minimized noise throughout the stimulation protocol. Dopamine signal was isolated from the background-subtracted voltammetric signal using chemometric analysis (Heien et al., 2005) with custom code for principle component regression (Keithley et al., 2009) written in MATLAB (MathWorks). Training sets for

this analysis included standard cyclic voltammograms of dopamine and pH changes obtained from optogenetic stimulation in DAT-cre mice expressing ChR2 in the VTA, as well as electrode-specific background drift from the current recordings (Howard et al., 2017; Keithley and Wightman, 2011). Dopamine concentration was estimated based on average post-implantation electrode sensitivity (Clark et al., 2010). Nissl staining was used to visualize lesion sites created following FSCV measurements. Briefly, 30 μm frozen vibratome sections were mounted on slides, air-dried and placed into 1:1 ethanol/chloroform overnight. Slides were then rehydrated through ethanol dilutions to distilled water, stained in 0.1% cresyl violet solution for 10 minutes. Slides were then rinsed with water and differentiated in 95% ethanol for 30 minutes and dehydrated in 100% ethanol for 2 × 5 minutes before being cleared in xylene 2 × 5 minutes and coverslipped.

In vitro FSCV

For recording electrodes, cylindrical carbon-fiber electrodes were prepared with 7 μm diameter fibers (~100 μm of exposed fiber, GoodFellow) inserted into a glass pipette (1.0 mm, A-M systems) and pulled to seal the pipette around the carbon-fiber. The electrode was held at −0.4 V versus Ag/AgCl and a triangular voltage ramp (−0.4 to +1.3 at 400 $V.s^{-1}$) was delivered at 10 Hz. DA transients were evoked in the medial NAc shell by optogenetic stimulations (473 nm, 1 s, 5 ms pulse-width) at various frequencies (5-50 Hz) through the light path of the microscope. Data were collected and analyzed using TarheelCV software. The amplitude of DA transients was measured from the oxidation peak region and 3 responses were averaged. For positive control recovery experiments DA was prepared fresh daily and bath-applied at 10 μM for 10 min followed by bath application of ACSF (10 min, wash) prior to repeated DA measurement at the same recording site.

Behavioral studies

Behavioral pharmacology

Horizontal locomotor activity was measured in square plastic chambers (17 × 8.9 cm) using an automated video tracking system (ANY-maze, Stoelting Co.). The following drugs (all Sigma-Aldrich unless indicated) were injected: 50 $mg.kg^{-1}$ L-DOPA and 12.5 $mg.kg^{-1}$ benserazide (i.p.) in 0.25% (wt/ vol) ascorbate in PBS, d-amphetamine hemisulfate (5 $mg.kg^{-1}$, i.p.) in saline, SKF81297 (0.2 $mg.kg^{-1}$, i.p.; Tocris #1447) in saline. All drugs were injected at 10 $ml.kg^{-1}$ except for L-DOPA/benserazide, which was injected at 33 $ml.kg^{-1}$.

2-nosepoke self-stimulation

Mice were placed on a restricted feeding schedule: food restriction consisted of removing food the evening before the first day and *ad libitum* access was then restricted to a 3-h daily period following the assay. At the beginning of the session, ferrules were connected to a 50-mm optical patch cable connected to an optical commutator (Doric Lenses) and mice were placed in operant chambers (Med Associates) controlled by MedPC IV software. The start of the session was signaled by a brief tone (2 kHz, 1 s), illumination of overhead house light, and LED cue lights over the nosepoke holes; sessions lasted 45 min. The chamber contained two photobeam-equipped nosepoke holes which were each baited at the start of each session with a sucrose pellet (Bio-Serv, F0071). Beam-breaks on the active nosepoke led to a 0.5 s tone, the LED cue lights over the nosepokes turned off for the duration of the photostimulus, and the activation of a TTL-controlled DPSS laser (473 nm, Shanghai or OEM laser) set to deliver pulses at 10 mW (80 $mW.mm^{-2}$ at 200-m fiber tip) at 40 Hz (1 s, 10-ms pulse width) controlled by an Arduino stimulus generator. Laser power was measured using a digital power meter (Thorlabs PM100D/S121C). Nosepokes that occurred during ongoing photostimulation were recorded but were without effect; inactive nosepokes led to identical tone and cue light effects but did not trigger the laser.

Real-time place preference

On a baseline (pre-test) day, mice were placed on the border between two adjoining (20 × 20 cm) homogeneous gray compartments and the amount of time spent in each compartment was recorded using video tracking software (ANY-maze). On the subsequent day, one side was designated active, where entries triggered photostimulation (473 nm, 10 mW, 40 Hz, 10-ms pulse width) using the lasers as described above but controlled by an ANY-maze interface (San Diego Instruments). Sessions lasted for 30 min and the amount of time spent in each compartment and the number of crossings was recorded.

QUANTIFICATION AND STATISTICAL ANALYSIS

To evaluate statistical significance, data from Figures 1B, 1D, 4B, S1B, S1D, S2A–S2C, S3B, S3D, S3F, and S3H were subjected to Student's t tests (KyPlot). Data from Figures 1F, 1G, 2B, 2C, 2E, 2F, 3B, 3C, 3E, 3F, 4D–4G, S2A–S2C, S3C, and S3G were subjected to RM one- or two-way ANOVAs followed by Sidak or Tukey post hoc analysis (GraphPad Prism v6). Friedman nonparametric test was used for non-Gaussian-assumed data from Figure 1I. In all the figures data are presented as means ± SEM unless noted and statistical significance was set at $p < 0.05$.